

Networking across Boundaries: Enabling Wireless Communication through the Water-Air Interface

Francesco Tonolini and Fadel Adib
MIT Media Lab

ABSTRACT

We consider the problem of wireless communication across medium boundaries, specifically across the water-air interface. In particular, we are interested in enabling a submerged underwater sensor to directly communicate with an airborne node. Today's communication technologies cannot enable such a communication link. This is because no single type of wireless signal can operate well across different media and most wireless signals reflect back at media boundaries.

We present a new communication technology, *translational acoustic-RF communication (TARF)*. TARF enables underwater nodes to directly communicate with airborne nodes by transmitting standard acoustic signals. TARF exploits the fact that underwater acoustic signals travel as pressure waves, and that these waves cause displacements of the water surface when they impinge on the water-air boundary. To decode the transmitted signals, TARF leverages an airborne radar which measures and decodes these surface displacements.

We built a prototype of TARF that incorporates algorithms for dealing with the constraints of this new communication modality. We evaluated TARF in controlled and uncontrolled environments and demonstrated that it enables the first practical communication link across the water-air interface. Our results show that TARF can achieve standard underwater bitrates up to 400bps, and that it can operate correctly in the presence of surface waves with amplitudes up to 16 cm peak-to-peak, i.e., 100,000 \times larger than the surface perturbations caused by TARF's underwater acoustic transmitter.

CCS CONCEPTS

- Networks → Cyber-physical networks; Mobile networks; Sensor networks;

Permission to make digital or hard copies of all or part of this work for personal or classroom use is granted without fee provided that copies are not made or distributed for profit or commercial advantage and that copies bear this notice and the full citation on the first page. Copyrights for components of this work owned by others than the author(s) must be honored. Abstracting with credit is permitted. To copy otherwise, or republish, to post on servers or to redistribute to lists, requires prior specific permission and/or a fee. Request permissions from permissions@acm.org.

SIGCOMM '18, August 20–25, 2018, Budapest, Hungary

© 2018 Copyright held by the owner/author(s). Publication rights licensed to the Association for Computing Machinery.

ACM ISBN 978-1-4503-5567-4/18/08...\$15.00
<https://doi.org/10.1145/3230543.3230580>

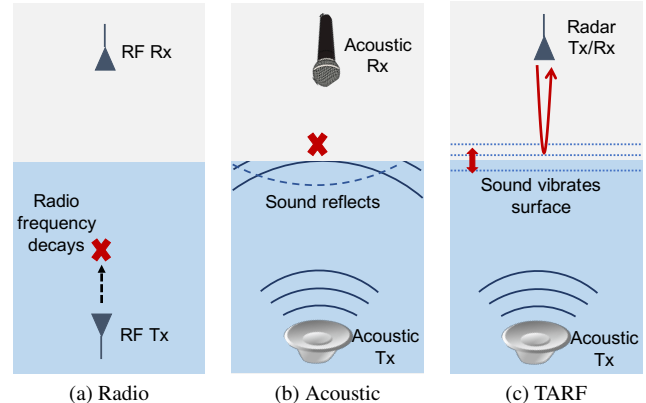


Figure 1—Enabling Communications across the Water-Air Boundary.
(a) shows that a radio transmitter cannot communicate because radio signals die exponentially fast in water. (b) shows that acoustic signals reflect off the water surface. (c) shows that a TARF receiver employs a radar to sense surface vibrations caused by acoustic pressure waves and use them for decoding.

KEYWORDS

Wireless, Subsea Internet of Things, Cross-Medium Communications

ACM Reference Format:

Francesco Tonolini and Fadel Adib. 2018. Networking across Boundaries: Enabling Wireless Communication through the Water-Air Interface. In *SIGCOMM '18: ACM SIGCOMM 2018 Conference, August 20–25, 2018, Budapest, Hungary*. ACM, New York, NY, USA, 15 pages. <https://doi.org/10.1145/3230543.3230580>

1 INTRODUCTION

Underwater communication networks all face the same problem: they cannot directly communicate across the water-air interface. Said differently, a deeply submerged sensor cannot directly communicate with another node above the water's surface [12, 13, 32, 52]. This is because wireless signals exhibit different properties in different media making it hard to use any single type of signal for cross-medium communications [12]. In particular, while radio waves can travel over long distances in air, they die exponentially fast in water (see Fig. 1(a)). Conversely, while acoustic waves can travel over long distances underwater, they reflect off the water's surface and hence cannot carry information across the water-air boundary (as shown in Fig. 1(b)).

Yet, enabling communication across the water-air boundary would bring benefits to numerous applications. In particular, offshore oil and gas exploration, ocean biological sensing,

and subsea Internet of Things (IoT) all need to establish communication links between underwater sensors and airborne nodes [8, 15, 32]. Today's state-of-the-art networks rely on autonomous underwater vehicles (AUVs) that act as data mules. These AUVs need to dive into deep sea to collect data from underwater sensors and continuously resurface to transmit collected data before diving back in. This makes the exploration process time-consuming and costly [18, 30], particularly in offshore oil exploration which require scanning vast areas of the seabed and where searching for and establishing a single deep-sea well can cost more than \$100 million [14]. Cross-medium communication also presents security challenges, which are particularly problematic in military applications. For example, to communicate with an airborne drone, a deeply submerged submarine needs to surface, compromising its location to an adversary [17, 23, 49].

A common approach to work around this problem has been to deploy relays that are partially submerged in water [37, 40, 57, 59]. The relays collect information from underwater nodes using acoustic links and relay it to nodes above the surface using radio signals. However, such relays can easily drift away with waves, severing communication to underwater sensors [59]. Moreover, this workaround leaves out submarines, which cannot rely on stationary deployed relays as they need to roam vast areas of the ocean.

We present TARP, the first system that enables deeply submerged underwater nodes to directly communicate across the water-air boundary by leveraging standard acoustic links. TARP's design exploits the fundamental physical properties of acoustic waves, as demonstrated in Fig. 1(c). In particular, an acoustic signal emitted by a sound transducer travels as a pressure wave. When the pressure wave hits the water surface, it causes a perturbation or displacement of the surface due to its mechanical nature. To pick up these signals, TARP relies on an airborne Radio Frequency (RF) sensor. The sensor transmits an RF signal and measures its reflection off the water surface. These reflections vary due to the surface displacement caused by the impinging acoustic signals from an underwater transmitter. TARP's receiver analyzes the variations in RF reflections and uses them to decode the bits communicated by an underwater node. We call this phenomenon *translational acoustic-RF (TARP) communication*, as it enables communication by leveraging a translation between acoustic signals and the RF reflections.

This new communication modality presents unique constraints due to the entanglement of both electromagnetic and mechanical nature of the resulting links, as well as unique environmental challenges. As a result, translating this communication paradigm into a practical networked system still faces multiple challenges:

- First, the surface vibrations caused by acoustic waves are very minute – of the order of few to tens of microns. The

displacement becomes even more shallow when the node is deeply submerged in the ocean.

- More importantly, these perturbations are easily masked by ocean waves that disturb the water surface and are three to six orders of magnitude larger than them.
- Finally, the underwater acoustic transmitter has no mechanism of estimating the overall channel. This makes it prohibitive to choose the right modulation and coding schemes to match the wireless channel quality. In particular, while the above design enables uplink communication, it remains elusive for the airborne sensor to send channel feedback to the underwater node since RF signals are not mechanical and hence will not vibrate the water's surface and translate into acoustic waves.

To overcome these challenges, TARP co-designs the transceiver architecture with the communication protocols. At a high level, it leverages a highly accurate RF-based sensor that can measure minute reflections and introduces new algorithms that can decode and eliminate unwanted interference. We highlight the different system components below:

- First, we employ a millimeter wave sensor as a receiver to capture and decode the RF reflections from the water surface. Specifically, TARP's airborne sensor transmits signals whose wavelength is few millimeters and measures the phase of their reflection. Due to the small wavelength, even surface displacements of few microns can lead to detectable phase changes of few degrees, allowing TARP to sense and decode very minute surface vibrations. We further incorporate the millimeter wave sensor into an FMCW (Frequency-Modulated Carrier Wave) radar, which allows it to focus its beam on the water surface, and mitigate noise and interference from undesired reflections.
- Second, we realize that ocean waves can be treated as structured interference in our context due to their mechanical nature, and design filters that can mitigate their impact on the received signal.
- Third, we discover unique properties of this new communication modality, which arise from the translation between pressure and displacement at the water-air interface. For example, we show that the channel's frequency-selective fading is inversely proportional to the transmit acoustic frequency. Our transmitter and receiver take these properties into account to design a power- and rate-optimal modulation scheme across the operational bandwidth.
- Finally, to select an appropriate bitrate, TARP can incorporate a pressure sensor as a proxy for the channel. The pressure sensor can be used to infer the distance to the surface and estimate the dominant pathloss component. This would allow a TARP transmitter to perform rate adaptation despite the lack of receiver feedback.

We built a prototype of TARP using underwater speakers and custom-made millimeter wave radars. We tested our

prototype in synthesized water tanks and a swimming pool (in the presence of practicing swimmers). Our experimental evaluation demonstrates the following results:

- Our prototype achieves cross-medium throughput of hundreds of bits per second in scenarios where existing communication technologies cannot establish any link.
- TARF can decode the transmitted packets even in the presence of waves by up to 8 cm of height (16 cm peak-to-peak), i.e., 100,000 \times larger than the (μ m) displacement caused by the transmitted acoustic signals.
- We empirically evaluate the communication link with different modulation schemes (BPSK, QPSK, 16-QAM, etc.), and we demonstrate that TARF’s channel-aware rate and power allocation algorithm can consistently outperform flat modulation schemes. Moreover at low SNRs, TARF’s adaptation scheme can improve the throughput up to 10 \times compared to flat modulation schemes.

While these results are promising, we believe they only represent a first demonstration of TARF’s capability as a cross-medium communication technology, and our design still exhibits multiple limitations. First, because our system cannot sustain a communication link in the presence of waves with amplitudes larger than 16 cm, it cannot operate under all weather conditions. In particular, it is resilient to capillary waves – which consist the dominant ocean surface wave on calm days – but not to wind waves. Another key limitation arises from the need to have the transmitter and the receiver relatively aligned along a vertical axis, since the throughput decays rapidly when they are misaligned (as we quantify in §8). Despite these limitations, we hope that this work can motivate researchers to explore and develop TARF to enable truly ubiquitous cross-medium communication, and allow underwater computing devices to seamlessly communicate with the outside world.

Contributions. TARF is the first communication technology that enables a deeply submerged underwater node to directly communicate with a compact airborne node. We present the design, prototype implementation, and evaluation of this technology demonstrating that it can achieve standard underwater data rates in scenarios where past technologies cannot establish any communication throughput.

2 RELATED WORK

TARF builds on past literature in two main areas: underwater communication networks and wireless sensing, as we detail below. In contrast to past work in these areas, TARF introduces the first system that leverages sensing as a means for communication across the water-air boundary.

Underwater Communication. The sinking of the *Titanic* in 1912 and the start of World War I spurred interest in underwater communication and sensing [35]. This led to the

development of SONAR systems, which leverage sound and ultrasonic signals for submarine communications and for detecting icebergs and U-boats [28, 35]. The appeal of acoustic communication arises from their low attenuation in water in comparison to RF signals. However, none of the early systems could communicate across the water-air boundary [35].

Interest in underwater communication and sensing resurfaced during the Cold War [25, 27]. The US and Soviet navies developed ELF (extremely low frequency) communication systems which operate at 30–300 Hz and are capable of communicating across the air-water boundary [9, 41]. The key challenge with these systems is that, due to their very long wavelengths, they require kilometer-long antennas, which make them infeasible to incorporate into underwater vehicles [41, 56]. As a result, most of the deployment of these systems remained limited to restricted point-to-point anchors deployed in specific locations [9, 41].

Over the past two decades, there’s been mounting interest in underwater networking for ocean exploration as well as oil and gas mining [14, 42, 54]. To overcome the water-air barrier, these systems rely on nodes that incorporate two communication modules: acoustic and RF [40, 41]. To send information across the air-water boundary, these nodes dive deep into the water to communicate with underwater sensors, typically deployed on the sea bed, collecting information from them using acoustic signals and re-surfacing frequently to relay this information using RF signals for in-air communication, before diving again to collect more data [36, 37, 48]. Significant research in the robotics community has focused on how to perform this process efficiently with robotic swarms or how to place partially-submerged relay nodes to optimize coverage [42, 48, 57]. Similarly, the military has deployed such relay nodes in permanent points of interest in the ocean [34]. However, these systems still suffer from the ability to scale, and are not feasible for submarines as surfacing would compromise their location. In contrast, TARF does not suffer from these problems as it enables submerged nodes to directly communicate through the water-air interface.

Finally, recent research has explored other means of underwater communication, including optics [31, 55] and quantum entanglement [26]. In contrast to TARF, the former has the same drawbacks of RF waves in its limited range [31, 55] and the latter is theoretical or still in the proof-of-concept phase.

Wireless Sensing. Over the past few years, the networking community has taken much interest in using communication signals for sensing purposes, e.g., sensing human locations, gestures, and vital signs [6, 7, 39]. Similarly, the radar community has explored wireless for sensing coarse water surface levels and surface currents [16]. TARF is inspired by these recent advances but differs in its goals, technique, and capabilities. Specifically, in contrast to past work on sensing,

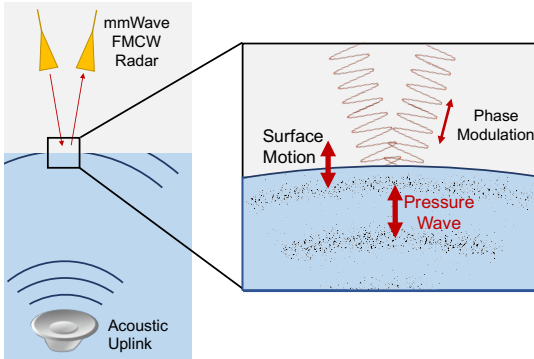


Figure 2—Surface Vibrations Translate into Phase Modulation. The phase of the wireless reflection changes with minute surface vibrations.

TARF introduces a new technique that leverages sensing *for* communication, particularly to enable communication across the water-air boundary. In terms of capabilities, due to its wavelength of operation, TARF can extract displacements of the order of few microns, i.e., at a scale three orders of magnitude finer than the millimeter-scale movements of past work [7, 10]. And finally, TARF builds on its basic idea of acoustic-RF translational communication to develop a full system that can address practical constraints including ocean waves and coupled RF-acoustic channels.

3 TARF OVERVIEW

TARF is a new communication technology that allows submerged underwater nodes to wirelessly communicate directly with nodes over the water’s surface. The communication link naturally consists of three components shown in Fig. 2:

- **Transmitter:** A TARF underwater node sends packets using a standard acoustic transducer (e.g., underwater speaker). The transmitter leverages signals in the 100-200 Hz frequency range, which are typically used for underwater communications by submarines and AUVs due to their low attenuation and long travel distances in water [44, 44, 45].
- **Channel:** The acoustic signal travels as a pressure wave inside the water. When the pressure wave hits the water surface, it causes a surface displacement that is proportional to the pressure wave.
- **Receiver:** TARF’s receiver consists of a millimeter-wave FMCW (Frequency Modulated Carrier Wave) radar. The radar transmits a wideband signal (centered around 60 GHz) and measures its reflection off the water’s surface. As the water surface vibrates due to the acoustic pressure waves, these vibrations modulate the phase of the reflected signal. The radar receiver extracts these phase changes and decodes them in order to recover the transmitted packets.

Scope. TARF focuses on the problem of uplink wireless communication between underwater and airborne nodes. Enabling such communication opens up capabilities in several areas:

- **Deep-sea Exploration:** Deployed underwater sensors could perform continuous monitoring and leverage TARF to send their collected information to the outside world. A drone may fly over large areas and collect information from a network of deployed underwater nodes.
- **Submarine Communication:** Submarines could leverage TARF to communicate with airplanes without the need for surfacing or compromising their locations.
- **Search and Recovery:** Finally, uplink communication can contribute to solving the long-standing problem of finding vehicles that go missing underwater (e.g., missing airplanes). In particular, TARF would enable these vehicles to continuously send distress signals to the surface, which can be picked up from the air, enabling rapid airborne search for lost or malfunctioning vehicles.

In what follows, we first explore the unique properties of TARF’s wireless channel in §4, then describe our design of TARF transmitter and receiver in §5 and §6 respectively.

4 UNDERSTANDING THE TARF COMMUNICATION CHANNEL

We start by analyzing TARF’s communication channel. The channel consists of three components: underwater propagation, the water-air interface, and in-air propagation. Since the underwater and in-air propagation components follow standard communication channels [33, 50], we focus our discussion on the water-air interface then incorporate our analysis into the end-to-end channel.

4.1 The Water-Air Interface

Recall that a TARF underwater transmitter sends packets using acoustic signals. These signals travel in the medium as pressure waves $P(r, t)$, which vary in time t and range r , and can be expressed as [33]:

$$P(\omega, t) = A(\omega)e^{j\omega(t-r/v_w)} \quad (1)$$

where A is the amplitude, ω is the angular frequency, and v_w is the velocity in water. Note that the amplitude A is also a function of distance r , but we omit it for simplicity.

Below, we first quantify the amount of surface displacement caused by these pressure waves, then describe how TARF can measure these displacements.

4.1.1 How much surface displacement do acoustic pressure waves create?

Acoustic pressure waves are longitudinal waves. As they propagate in a medium, they displace the medium’s particles along their same direction of travel. (Such particle displacement is similar to how particles of a spring move as it compresses and relaxes due to a pressure wave traveling through it.) Hence, when a pressure wave hits the surface of water, it also causes a surface displacement δ . This displacement can be computed

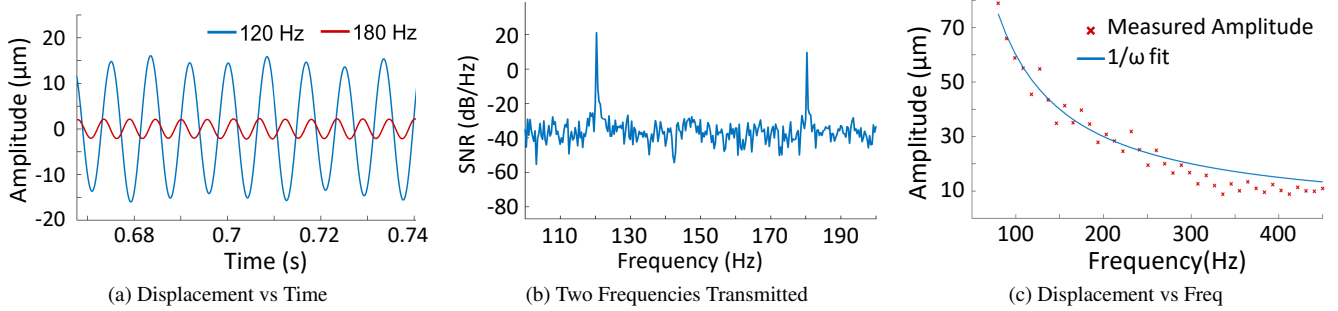


Figure 3—Understanding the Surface Displacement as a Function of the Acoustic Pressure Wave. (a) shows the displacement over time when a single frequency is transmitted, at a frequency of 120Hz and at a frequency of 180Hz. (b) shows the absolute value of the fourier transform of the power amplitude when the same two frequencies are transmitted simultaneously. (c) shows the amplitude of the displacement as a function of the frequency of the acoustic signal.

by solving the boundary conditions of the wave equation. In the interest of brevity, we include the solution below and refer the interested reader to [51] for a derivation. Assuming the incident wave is orthogonal to the surface, we can derive:

$$\delta(\omega, t) = \frac{P(\omega, t)}{\rho_w \omega v_w} \quad (2)$$

where P is the overall pressure created by the acoustic wave and ρ_w is the density of water.

To better understand this relationship, we perform experiments with an underwater speaker. We use the Electro-Voice Underwater Speaker [1], place it about half a meter below the surface of water, and point it upward toward the surface in a setup similar to that shown in Fig. 2. The speaker transmits an acoustic signal, and we measure the displacement at the surface of the water.¹

We perform three types of experiments. First, we transmit a single tone from the speaker, first at a lower and then a higher frequency, and plot the measured displacement in Fig. 3(a). Next, we transmit two tones simultaneously from the speaker and plot the fourier transform of the resulting displacement in Fig. 3(b). And finally, we run an experiment where we vary the frequency of the transmitted tone over time and plot the peak-to-peak displacement in Fig. 3(c).

Based on these figures, we observe the following:

- *The displacement caused by the pressure wave is very minute:* Fig. 3(a) shows that the peak-to-peak displacement is of the order of a few μm to a few tens of μm , even though the underwater transmitter was only submerged half a meter below the water’s surface.
- *The water-air interface acts as a linear channel in the context of TARP communication:* In particular, the frequency of the surface displacement matches the frequency of the transmitted acoustic signals by the underwater speaker in Fig. 3(a)-(b). Such behavior is in line with Eq. 2, which shows that the displacement is directly proportional to the pressure wave. This means that the water-air interface acts as a linear (and time-invariant) channel. Such channels

are amenable to different modulation schemes (AM, FM, BPSK, OFDM, etc.) and can be estimated with preamble symbols and inverted for reconstruction and decoding.

- *The amplitude of the displacement is inversely proportional to the frequency of the transmitted acoustic signal:* This can be seen through the $1/\omega$ decay in Fig. 3(c), which matches the expected behavior in Eq. 2. This property implies that lower frequencies are more desirable for TARP communication as they will cause a larger displacement, and hence a larger signal-to-noise ratio (SNR). It also implies that signals at different frequencies experience very different attenuation and that an optimal communication protocol should account for this unique feature of the channel.

4.1.2 Why can't we rely on acoustic signals alone?

Since the acoustic wave hits the surface and causes a displacement, the displacement itself can generate a pressure wave that travels in air. Hence, we ask whether it would be more efficient to directly leverage the generated pressure wave in the air for communication.

There are multiple reasons why such an approach is undesirable. First, while part of the pressure wave indeed crosses the boundary and travels in air, the majority of the incident pressure wave reflects off the water-air interface. In particular, by solving the sound wave equation for a wave incident at a boundary between two different media, we obtain the following relationship between the amplitude of the reflected wave A_r and the amplitude of the incident one A_i [33]:

$$A_r = \frac{v_a \rho_a - v_w \rho_w}{v_a \rho_a + v_w \rho_w} A_i. \quad (3)$$

where v_a and v_w are the speeds of sound in air and water respectively and ρ_a and ρ_w are the air and water densities. Due to the large difference between the constants for air and water, the reflected amplitude is almost equal to the incident one (i.e., $A_r \approx A_i$). And, by the law of conservation of energy, the amplitude of the transmitted signal $A_t = \sqrt{A_i^2 - A_r^2}$. Using standard values for velocity and density [60], we can show that pressure waves crossing into air attenuate by around 30dB solely because of reflection at the boundary.

¹Note that for measuring the displacement, we use the millimeter-wave radar we built as described in §7.

Second, aside from the attenuation at the boundary, acoustic waves experience exponential attenuation when traveling in air [33]. This makes them an unsuitable means for wireless communication over the air. Indeed, this is why wireless communication systems like WiFi and cellular employ RF signals instead of ultrasonic/acoustic signals.

4.1.3 Why can't we leverage the water-air interface for downlink communication?

So far, our discussion has focused on uplink communication. A natural question is: why can't we use the same technique to enable an in-air node to communicate with an underwater hydrophone. In principle, an acoustic signal transmitted from an airborne speaker should also cause a vibration of the water-air interface that can be picked up by an underwater hydrophone.

The answer lies in the nature of interference between the incident and reflected pressure waves at the water-air boundary. Specifically, these waves constructively interfere when they hit the boundary of a less dense medium (i.e., when traveling from water to air), but destructively interfere when they hit the boundary of a more dense medium (i.e., when traveling from air to water). Since the displacement is directly proportional to the overall pressure as per Eq. 2, the displacement is maximized for underwater pressure waves, but it is nulled for acoustic signals arriving from the air. Hence, while this mechanism enables underwater-to-air communication, it cannot enable an air-to-underwater communication link.

4.2 End-to-end TARP Channel

Now that we understand the water-air interface, we would like to quantify the impact of each of the channel components on the overall signal attenuation:

- *Underwater Propagation.* The attenuation of acoustic signals traveling underwater can be described by $e^{-\gamma r}/r$ where r is the depth and γ quantifies the absorption. This equation shows that the amplitude of the acoustic pressure wave decays exponentially as it travels underwater.
- *Water-Air Interface.* The attenuation at the water-air interface is given by Eq. 2 in terms of pressure. Assuming that the received power is proportional to $\delta(\omega, t)^2$, and knowing that the transmitted power is proportional to $P(\omega, t)^2$ and inversely proportional to ρ_w and v_w [11], we can express the sensed power at the water-air interface as:

$$P_{\text{sensed}} \propto \frac{P_{\text{incident}}}{\rho_w v_w \omega^2} \quad (4)$$

- *In-Air Propagation.* A standard radar signals attenuates as $1/d_0^2$, where d_0 is the distance between the transmitter and the receiver [47].² However, because water is specular at the wavelengths of RF signals (i.e., it reflects back all the impinging RF signals) [19], we can approximate the overall signal attenuation as $1/(2d_0)$.

²Power decays as $1/d_0^4$, but the signal amplitude attenuates as $1/d_0^2$.

Given the above breakdown, the overall pathloss (PL) in dB is linear in depth r and logarithmic in height d_0 , density ρ_w , frequency ω , and velocity v_w . Since ρ_w and v_w are known,³ estimating the overall attenuation requires estimating only r and d_0 . Further, since the path loss increases linearly in r but logarithmically in d_0 , the dominant unknown path loss component is expected to be r . In §5, we explain how TARP can estimate this component.

5 DESIGNING A TARP TRANSMITTER

In this section, we describe how TARP's acoustic transducer encodes and modulates its transmissions by taking into account the properties of the TARP communication channel.

5.1 What is the right modulation scheme?

Recall that TARP's channel is amenable to various modulation schemes since it is linear and time-invariant. The channel, however, is highly frequency selective, as can be seen in Fig. 3(c). Such frequency-selective fading leads to inter-symbol interference, which complicates the receiver design.

To deal with such frequency-selective fading, TARP employs Orthogonal Frequency Division Multiplexing (OFDM) as an encoding scheme at its transmitter. OFDM is widely used in WiFi and LTE systems. In what follows, we briefly describe how OFDM works and refer the interested reader to [60] for more information.

Instead of encoding the transmitted bits directly in the time domain, an OFDM transmitter encodes symbols in the frequency domain. For example, if we consider each frequency in Fig. 3(c) as a subcarrier, an OFDM transmitter can treat each frequency as an independent channel and transmit flows on all of them concurrently. The OFDM encoding scheme is attractive because decoding can be done in the frequency domain without the need for complex channel equalizers.

5.2 What is the optimal power allocation?

Next, we ask how should a TARP transmitter divide its power across the different subcarriers? According to Fig. 3(c), a TARP channel has high SNR at lower frequencies and lower SNR at higher frequencies. With this knowledge, it is clear that distributing the power evenly across the different subcarriers would result in sub-optimal performance. Conversely, a power allocation strategy that concentrates all the available power into the lowest-frequency subcarrier would maximize the SNR, but also result in sub-optimal performance since it forgoes much of the available bandwidth.

Optimal power allocation is a well-studied problem in information theory [50]. The generic solution for this problem

³Note that these parameters depend on the water salinity and temperature, which we assume the underwater sensor can directly estimate or infer.

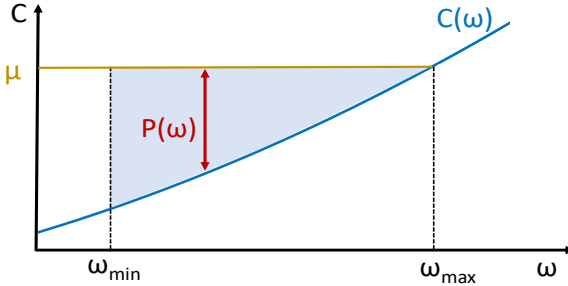


Figure 4—TARF’s Waterfilling. The noise $C(\omega)$ increases with frequency ω . The level μ determines the optimal power allocation (shaded region), where $P(\omega)$ denoting the power at every frequency.

is called waterfilling. In what follows, we describe this concept in the context of a TARF communication channel and highlight why it is particularly interesting in this context.

Fig. 4 plots the noise power $C(\omega)$ in blue as a function of frequency ω . As per Eq. 4, we can express $C(\omega) = \rho_w v_w \omega^2 / a$, where a is a real positive constant which depends on the transmitted signal power, the distance attenuation, and the receiver noise floor. The high level idea of waterfilling is that we can solve for a water level μ , depicted by the yellow line in Fig. 4. Specifically, the optimal power allocation is the difference between μ and the noise power $C(\omega)$. We can express the optimal power allocation as:

$$P(\omega) = \begin{cases} \mu - C(\omega), & \text{if } \mu - C(\omega) \geq 0 \\ 0, & \text{otherwise} \end{cases} \quad (5)$$

So how can we find μ ? To solve for μ , we use the total power constraint, which states that the total power across all the subcarriers (i.e., the integral of the power densities) must equal the total power of the transmitter P_0 .

$$\int_{\omega_{min}}^{\infty} P(\omega) d\omega = P_0 \quad (6)$$

In our context, ω_{min} is the lowest frequency at which the underwater speaker or acoustic transducer can operate.

In general, because of the non-linear nature of Eq. 5, the water filling problem is solved numerically. However, in the context of a TARF channel, the function $P(\omega)$ is continuously decreasing, meaning that the above integral can be computed without the non-linearity over the interval in which it is positive. Such interval spans from ω_{min} to the frequency at which the power density $P(\omega)$ is equal to zero, ω_{max} as shown in Fig. 4. Setting Eq. 5 to zero and solving for ω we get $\omega_{max} = \sqrt{\frac{a\mu}{\rho_w v_w}}$. Using this maximum frequency and the total power constraint of Eq. 6, we obtain the following third degree polynomial in $\sqrt{\mu}$:

$$\frac{2}{3} \sqrt{\frac{a}{\rho_w v_w}} \mu^{\frac{3}{2}} - \omega_{min} \mu + \frac{\rho_w v_w \omega_{min}^3}{3a} - P_0 = 0. \quad (7)$$

The real positive root of this polynomial gives the level μ which allows us to obtain an analytical form for the optimal

power distribution with respect to the noise frequency profile discussed above. The TARF transmitter uses this information to assign power to its subcarriers according to this computed distribution at the center frequency of each subcarrier.

5.3 How to modulate the subcarriers?

Recall that in OFDM-based systems, we can treat each subcarrier as a separate flow with its own modulation (BPSK, QPSK, etc.). After TARF determines the optimal power allocation, it proceeds to bitrate selection on a per-subcarrier basis.

Specifically, knowing the power allocation $P(\omega)$ and the noise function $C(\omega)$, TARF can estimate the expected SNR at the receiver and choose the appropriate bitrate based on its estimate. In particular, it can leverage higher modulations (e.g., 64-QAM) at lower-frequency subcarriers (which have higher SNRs) and lower modulation schemes (e.g., BPSK) at higher-frequency subcarriers (which have lower SNRs).

- We note few more points about TARF’s bitrate selection:
- The exact SNR at which TARF should switch between the different modulation schemes can be determined both analytically and empirically. In §8, we describe how TARF’s empirical evaluation matches the analytical solution.
 - Our discussion above focused on performing rate adaptation by only changing the modulation scheme. In practice, the discussion can be extended to adapting the coding rate (e.g., 1/2-rate or 3/4-rate coding) as well [38].
 - Finally, in order for a receiver to decode transmitted packets, it needs to know the modulation scheme employed by every subcarrier. Such information is typically embedded in the packet header which is sent via BPSK modulation.

5.4 How to adapt the bitrate?

So far, our discussion has assumed that TARF’s transmitter has perfect knowledge of the noise function $C(\omega)$. Unfortunately, however, TARF does not have direct access to channel information. This is because TARF can only perform one-way communication; hence, the receiver is unable to send the channel estimates as feedback to the transmitter. To accommodate for channel uncertainty and frequency-selective fading, one-way communication systems are typically conservative: They choose modulation schemes with very low bitrate and large redundancy. For example, a GPS transmitter spreads every bit over 1024 chips and repeats each symbol 20 times.

To overcome this challenge, a TARF transmitter can leverage known properties of the channel and combine them with side-channel information. In particular, recall from §4.2 that the only unknown components of the attenuation are the height above the water d_0 and the depth of the TARF transmitter r . Hence, if TARF can estimate these components, then it would be able accurately estimate the overall SNR.

To estimate the depth underwater, a TARF transmitter can employ a pressure sensor. In particular, underwater pressure

Algorithm 5.1 Transmitting through a Tarf Channel**POWER ALLOCATION**

▷ Path Loss Estimation

Estimate depth; $r \leftarrow p/\rho_{wg}$ Estimate path-loss $PL(\omega)$ from §4.2

▷ Power Distribution

Solve for level μ from Eq. 7Compute power allocation: $P(\omega) \leftarrow (\mu - C(\omega))^+$ **MODULATION**

▷ SNR Estimation

Estimate SNR per subcarrier: $SNR(\omega) \leftarrow P(\omega) \times 10^{PL(\omega)/10}$

▷ Modulation

if $SNR(\omega) <= SNR_1$ $Mod(\omega) \leftarrow BPSK$ *elseif* $SNR_1 < SNR(\omega) <= SNR_2$ $Mod(\omega) \leftarrow QPSK$ *elseif* $SNR_2 < SNR(\omega) <= SNR_3$ $Mod(\omega) \leftarrow 16QAM$ *else* $Mod(\omega) \leftarrow 64QAM$ **TRANSMISSION**

▷ Add preamble, cyclic prefix, CRC

▷ Transmit

can be directly mapped to depth (through $P = \rho_v gr$, where ρ_v is the density and g is the gravitational field strength). In fact, today's off-the-shelf pressure sensors have millimeter-level precision in measuring underwater depth [53].

This leaves Tarf only with the height of the receiver as an unknown. In practical scenarios, the transmitter may have prior knowledge of the receiver's height. For example, underwater submarines trying to communicate with airplanes can have reasonable estimates on the altitude at which airplanes fly based on standard flight patterns. Alternatively, the plane may decrease its altitude to improve its SNR to an underwater submarine communicating with it via Tarf. In the case of subsea IoT, the expected height can be provided to a sensor prior to deployment. We summarize the overall procedure of a Tarf transmitter in Alg. 5.1.

Finally, one might wonder whether Tarf's transmitter could employ rateless codes instead of its bitrate adaptation scheme. Unfortunately, rateless codes still require feedback from the transmitter (in the form of acknowledgments) [20, 21], which is still not possible given the uplink-only constraint on a Tarf communication link. In contrast, Tarf's transmitter can adapt its bitrate by exploiting side channel information despite this constraint.

6 DESIGNING A TARF RECEIVER

In this section, we describe how we design a Tarf receiver. We start by describing how the receiver can measure the

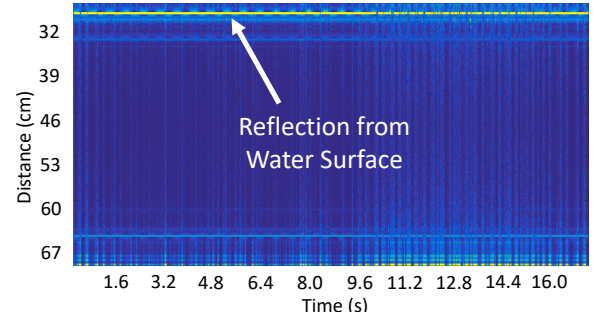


Figure 5—Capturing the Surface Reflection. The FMCW spectrogram plots the power at each distance bin over time. The yellow line indicates the high power reflection arriving from the water surface.

minute surface displacements, then we discuss how it cancels interference caused by the ocean waves, and finally how it can decode the filtered reflection.

6.1 How can Tarf capture the minute surface displacements?

Recall that Tarf's receiver employs a radar to capture the surface vibrations caused by the acoustic pressure waves. The radar transmits an RF signal and measures its reflection off the water surface. Given the very minute (μm -scale) displacement at the surface of the water, leveraging time-of-flight based techniques to directly measure the displacement would require few THz of bandwidth (since bandwidth is inversely proportional to the resolution).⁴

Instead of trying to directly estimate the distance, Tarf measures the *change in distance* by estimating the phase of the reflected signal. In particular, the phase of the reflected radar signal $\phi(t)$ can be expressed as:

$$\phi(t) = 4\pi \frac{d_0 + \delta(t)}{\lambda} \quad (8)$$

where d_0 is the distance between the radar and the water surface (in the absence of vibrations) and λ is the wavelength of the radar's transmitted signal.

The above equation reveals three important observations:

- First, Tarf's ability to track the surface displacement is strongly impacted by its choice of the wavelength λ . On one hand, a relatively large wavelength (e.g., few centimeters as in WiFi or cellular) would result in very minute variations in the phase, making it less robust to noise. On the other hand, choosing a very small wavelength (e.g., sub- μm as in THz or optical frequencies) would result in rapid phase wrapping, precluding the ability to track the surface vibrations.
- Second, the choice of wavelength λ also impacts Tarf's ability to adapt to ocean waves in the environment. In particular a very small wavelength will suffer from rapid phase rotation even in the presence of very small waves.

⁴The resolution is $c/2B$ where c is the speed of light and B is the bandwidth.

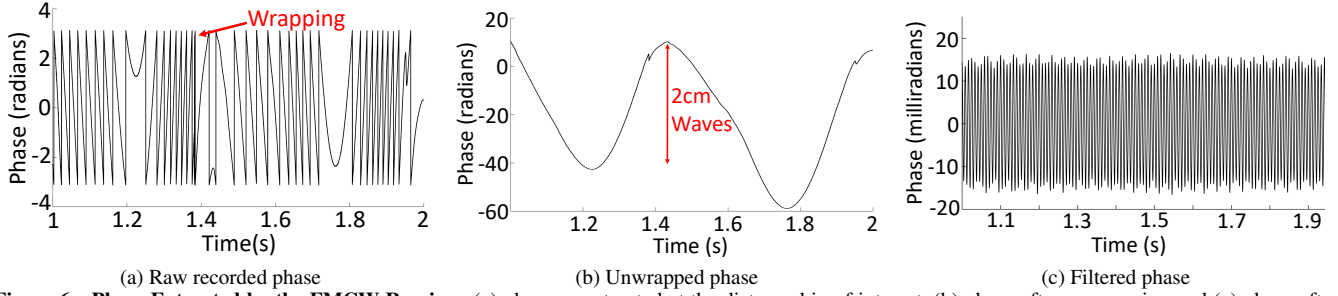


Figure 6—Phase Extracted by the FMCW Receiver. (a) phase as extracted at the distance bin of interest, (b) phase after unwrapping and (c) phase after applying a band pass filter to isolate the (communication) frequencies of interest.

- Third, because the phase of a reflection is not robust to interference, TARP requires a more sophisticated sensing technology than a simple Doppler or phase-based radar.

To address these issues, the TARP receiver leverages a millimeter-wave Frequency Modulated Carrier Wave (FMCW) radar. In the rest of this section, we describe how the receiver employs the radar and highlight why millimeter wave frequencies offer a sweet spot for the operation wavelength.

6.2 How does FMCW extract the information of interest?

In order to achieve high phase resolution while mitigating interference from other reflectors in the environment, TARP leverages an FMCW-based wideband radar. At a high level, the wideband radar can filter the reflections coming from different distances into different bins. This enables it to isolate the reflection off the water’s surface from other reflections in the environment, and zoom in on its phase in order to decode the surface vibrations. In what follows, we describe the operation of the receiver in three main steps: surface reflection identification, phase extraction, and decoding.

6.2.1 Surface Reflection Identification

To explain the operation of TARP’s receiver, we run an experiment with the radar placed above the water’s surface in a manner similar to Fig. 2 such that it can capture the reflection off the water surface. We configure TARP’s underwater acoustic transmitter to transmit a single tone at 100Hz. The radar transmits a signal and measures its reflections. It can then process these reflections to obtain the power of the reflections as a function of distance. (For a thorough explanation of how it performs this processing, we refer the reader to [6].)

Fig. 5 plots the output of TARP’s FMCW processing as heatmap, where navy blue indicates low reflection power and yellow indicates high reflection power. The x-axis shows time, while the y-axis indicates the distance. A horizontal line indicates a reflection arriving from a particular location. Note that the different light blue patterns over time are due to noise.

To identify the reflection bin corresponding to the water surface, TARP exploits the fact that the water surface has the

largest radar cross section, and hence the highest reflection power. In Fig. 5, this corresponds to the solid yellow line.

6.2.2 Phase Extraction and Wave Elimination

Next, TARP zooms in on the phase of the range bin where it has identified the water reflection. Fig. 6(a) plots the phase of that bin as a function of time. Note that the phase in this figure wraps around every 0.2 s. This indicates a phase displacement larger than 5 mm (i.e., the wavelength of our millimeter wave radar). This phase wrapping arises from the waves at the surface of the water, whose presence masks the μm -scale vibrations from the acoustic transmitter.

To eliminate the impact of these waves, TARP first unwraps the phase. We plot the output of the unwrapped phase over time in Fig. 6(b). The waves exhibit a peak-to-peak variation of 50 radians. Given a wavelength of 5 mm, this corresponds to a 2cm peak-to-peak displacement, as per Eq. 8.

Next, to eliminate the impact of the waves, TARP filters the unwrapped phase and plots the output in Fig. 6(c). Note that in order to visualize the phase variations, the axis of this figure is zoomed in both in time and amplitude. Upon filtering the ocean waves, we can now see the single-tone transmitted by TARP’s underwater speaker at 150 Hz. Note that TARP can always filter out ocean waves since their frequency is significantly lower than its range of operation. Specifically, ocean waves typically range between 0.1Hz – 3Hz [43] while TARP’s transmitter operates above 100 Hz.

The above description demonstrates why using millimeter-wave frequencies offers a sweet spot for TARP communication. Specifically, they enable a TARP receiver to overcome (unwrap and filter) the impact of ocean waves while at the same time sensing surface displacements (of the order of few μm) due to underwater acoustic pressure waves.

6.2.3 Decoding

Our above experiment was conducted by configuring the underwater speaker to transmit a single frequency. In practice, however, a TARP transmitter sends OFDM symbols over its bandwidth of operation as described in §5. To decode these symbols, TARP’s receiver performs standard OFDM packet detection, extracts the channel and the modulations from the header, and uses them to decode the packet payload.

7 IMPLEMENTATION & EVALUATION

7.1 Implementation

Our prototype implementation of TARF consists of an underwater acoustic speaker as a transmitter and an airborne millimeter wave FMCW radar as a receiver.

(a) Acoustic Uplink. We implemented TARF’s uplink transmitter using an underwater speaker, namely the Electro-Voice UW30 Underwater Loudspeaker [1]. The speaker was connected to the output audio jack of a Lenovo Thinkstation PC through a power amplifier. In our evaluation, we used two types of amplifiers: the OSD 75W Compact Subwoofer Amplifier [2] and the Pyle 300W Stereo Receiver [3]. TARF’s transmit power levels are comparable to standard low power acoustic transducers used in underwater communications [46]. We configure the speaker to transmit signals over a bandwidth of 100Hz between 100Hz and 200Hz. Such bandwidth is typical for underwater communication systems [60].

TARF’s transmitter encodes its data using OFDM modulation. Each OFDM symbol consists of 64 subcarriers which cover the available bandwidth. The transmitter performs per-subcarrier power allocation and bit-rate adaptation as described in §5. Each OFDM symbol is pre-pended with a cyclic prefix, as in prior proposals that perform per-subcarrier bitrate adaptation [38].

Unless otherwise noted, in each experimental trial, we transmit 10 back-to-back OFDM symbols (two symbols act as a preamble and 8 as payload). The transmitter can include the modulation scheme for every subcarrier in its header, and a CRC for every subcarrier to determine whether the packet was received correctly.

(b) Millimeter-Wave FMCW Radar. We implemented TARF’s receiver as a custom-built millimeter-wave FMCW radar. To generate the desired millimeter-wave signals, we first generate a reference FMCW signal using a design similar to that implemented in [6]. The reference outputs a frequency ramp with a center frequency of 8.65GHz and a bandwidth of 500MHz. We feed the output of this FMCW signal generator into a $2\times$ frequency multiplier, whose output is in turn fed as a local oscillator to an off-the-shelf millimeter wave transmitter and receiver. This architecture enables transmitting and receiving an FMCW signal with a center frequency of 60GHz and a bandwidth of 3GHz. This results in an effective range resolution of 5 cm, and a phase sensitivity of $1.25\text{rad}/\text{mm}$. The millimeter wave transmit and receive boards are connected to 23 dBi horn antennas [4].

We programmed our FMCW generator to sweep its bandwidth every $80\mu\text{s}$. The receiver captures and downconverts the reflected signals to baseband and feeds them into a USRP N210 software radio [5] equipped with an LFRX daughterboard. The USRP digitizes the signals and sends them over

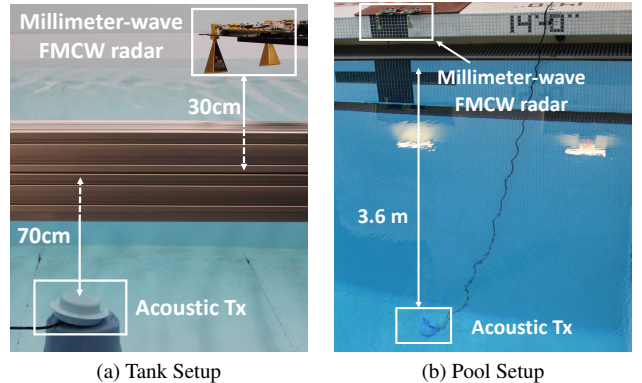


Figure 7—Experimental Setups. (a) shows the tank setup, with the acoustic transmitter placed 70 cm below the surface. (b) shows the pool setup, where we experimented with different depths. In both setups, the millimeter-wave radar was placed around 30 cm above the water surface and pointed downwards to record the acoustic vibrations.

an ethernet cable to a 64-bit machine running Ubuntu 16.04 for post-processing.

We implemented TARF’s decoder in MATLAB. The decoder identifies the range bin corresponding to the water surface as described in §6, then extracts the phase of the reflection and performs unwrapping and filtering. To decode the filtered phase signal, it performs packet detection, channel estimation, and decoding similar to a standard OFDM decoder.

7.2 Evaluation

We evaluated TARF in controlled and uncontrolled settings. We tested it in two environments: an enclosed water tank and a swimming pool during normal activity.

(a) Water Tank. Most of our evaluation was performed in a water tank of 1.3m depth and $3\text{m} \times 5\text{m}$ rectangular cross section, as shown in Fig. 7(a). In these experiments, we varied the height of the radar between 20cm and 40cm above the water surface, and varied the depth of the speaker between 5cm and 70cm. We also experimented with different locations across the tank and with different acoustic transmission levels.

To evaluate the robustness of TARF to waves, we manually generated the waves with a floating object and measured their peak-to-peak amplitude with a graded ruler at the water surface directly above the speaker.

(b) Swimming Pool. To evaluate TARF in a less controlled environment and at greater depths, we performed experiments in a swimming pool during normal activity. Fig. 7(b) shows our experimental setup. In our experiments, we placed the radar 30cm above the water surface and submerged the acoustic transmitter at depths between 90cm and 3.6m. During our experiments, the water surface was continuously disturbed by swimmers and circulation vents, enabling us to evaluate TARF’s robustness to environmental challenges.

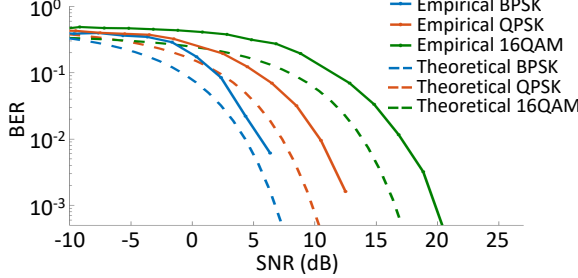


Figure 8—Per-subcarrier BER vs SNR. The figure plots the per-subcarrier BER against SNR for BPSK, QPSK and 16QAM modulations. The dashed lines show the theoretically predicted behavior for each modulation.

8 RESULTS

8.1 Performance

To evaluate TARP as a communication modality, we performed controlled experiments in the water tank setup described in §7.2 and measured TARP’s throughput across the water-air interface.

We performed 500 experimental trials in total. We varied the location and height of TARP’s transmitter and receiver as described in §7.2. We tested TARP in four configurations: the first three employ uniform power distribution and modulation across all the OFDM subcarriers using BPSK, QPSK and 16QAM. The final configuration incorporates TARP’s power allocation and rate adaptation schemes.

(a) BER-SNR curves. The performance of a wireless receiver can be evaluated through plots of the bit error rate to the signal to noise ratio, called the BER-SNR curves [22, 38]. We computed the BER as the fraction of correctly decoded bits to total transmitted bits. We computed the signal power as the squared channel estimate, and computed the noise power as the squared difference between the received signal and the transmitted signal multiplied by the channel estimate.

Fig. 8 plots the BER-SNR curves of TARP with BPSK (in blue), QPSK (in red), and 16-QAM (in green) modulations and compares them to the theoretical BER-SNR curves of the respective modulation schemes (in dashed lines) [22]. We make the following observations:

- TARP’s BER-SNR curves follow a similar trend to the theoretical ones. These trends demonstrate that TARP presents a viable cross-medium communication channel.
- Similar to standard communication systems, conservative modulation schemes (e.g., BPSK) maintain lower BER at the same SNR. This is expected since more conservative schemes allocate more power for every bit.
- There is a discrepancy between TARP’s performance and a theoretically optimal decoder. This can be explained by the fact that TARP’s decoder is not ideal and its channel estimation is not perfect.

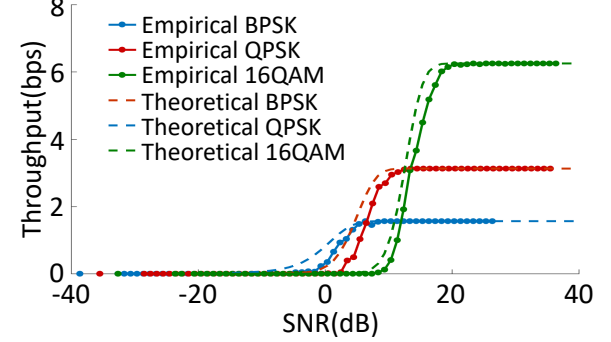


Figure 9—Per-subcarrier Throughput vs SNR. The figure plots the per-subcarrier throughput against SNR for BPSK, QPSK and 16QAM. The dashed lines show the theoretically predicted behavior for each modulation.

(b) Per-subcarrier Throughput-SNR curves. Recall that TARP multiplexes independent flows across OFDM subcarriers as described in §5. We are interested in evaluating the throughput versus per-subcarrier SNR. In our evaluation, we compute the throughput as the average number of correctly decoded packets (multiplied by bits per packet) at each SNR.

Fig. 9 plots the per-subcarrier throughput versus the SNR. The figure shows empirical results for BPSK (in blue), QPSK (in red), and 16-QAM (in green) and compares them to the theoretical throughput-SNR curves (plotted with dashed lines). We make the following remarks:

- Similar to our BER-SNR curves from §8.1(a), these per-subcarrier throughput-to-SNR curves follow a similar trend to the theoretical ones. This further confirms TARP as a viable communication channel.
- Also similar to the BER-SNR curves, there is a discrepancy between the empirical and theoretical curves. We observe that this discrepancy is more pronounced at lower SNRs, an observation that can be explained by less perfect channel estimation at the lower SNRs.
- The figure shows that for lower SNRs, higher modulations can achieve higher throughput. This demonstrates the need for TARP’s rate adaptation technique.

(c) Aggregate Throughput-SNR curves. Next, we evaluate TARP’s overall throughput performance as a function of overall SNR. The overall throughput is computed by summing the per-subcarrier throughput across all the subcarriers. The overall SNR is computed as the total signal power across all subcarriers divided by the total noise power across the subcarriers. For fair comparison to TARP’s power and rate adaptation scheme, we plot the achieved throughput as a function of the SNR computed prior to TARP’s power allocation.

Fig. 10 plots TARP’s overall throughput for the flat modulation schemes: BPSK (in green), QPSK (in red), 16-QAM (in blue) as well as with the adaptive modulation scheme from §5 (in black). We make the following observations:

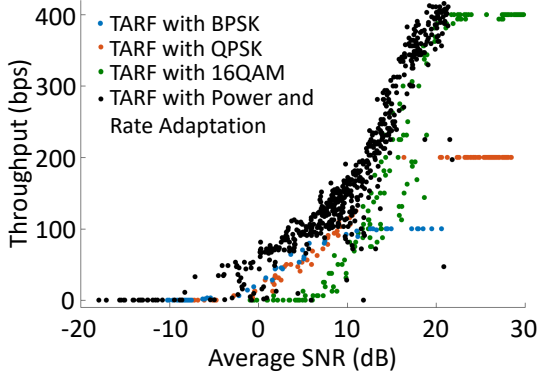


Figure 10—Throughput vs Average SNR. TARF’s power and rate adaptation achieves higher throughput than uniform power allocation and outperforms flat modulations.

- TARF can achieve throughputs of 100 bps, 200 bps and 400 bps for BPSK, QPSK and 16-QAM modulation respectively. This can be explained by the 100Hz bandwidth and the corresponding modulation schemes. These throughputs are similar to standard communication rates for underwater acoustic communication links [46].
- TARF’s power and rate adaptation consistently outperforms flat modulation schemes. This is due to two reasons: optimal power allocation and adapting the modulation for each channel to the per-subcarrier SNR.
- TARF’s benefits are particularly significant in low SNR regimes, which represent the prevailing scenario of underwater communication. Specifically, at an SNR of 0 dB, TARF’s rate and power adaptation can achieve about 10× throughput increase over any of the flat modulation schemes. This emphasizes the need for power and rate adaptation in a TARF communication link.

8.2 SNR Microbenchmarks

Next, we are interested in studying the SNR trends of TARF as a function of different parameters. In particular, we would like to quantify the impact of depth (of the underwater transmitter) and alignment (between the transmitter and the receiver) on the SNR of the received signal.

(a) SNR vs Depth. To understand the impact of depth on SNR, we evaluated TARF in the swimming pool setup described in §7. We placed the FMCW radar 30 cm above the water surface at the edge of the pool, and varied the depth of the underwater speaker between 90 cm and 3.6 m. We overpowered the speaker with the Pyle 300W Stereo receiver and configured it to transmit a single tone at 150 Hz, and we measured the resulting surface vibration using the radar. We performed 45 three-second trials across the different depths.

Fig. 11 shows our results. The figure plots the mean and standard deviation of the received signal as a function of distance (in orange). We make the following observations:

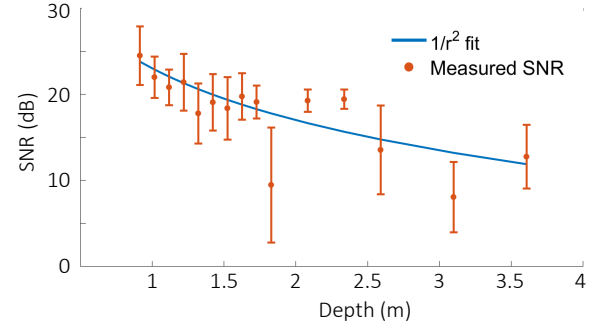


Figure 11—SNR vs Transmitter Depth. The figure shows that TARF’s SNR decreases with depth (in orange) following a $1/r^2$ trend (in blue). It outperforms pure RF links which decay exponentially in distance underwater. Error bars indicate standard deviation.

- The SNR decreases from around 25 dB at 90 cm to 14 dB at 3.6 m. The SNR trend follows a $1/r^2$ curve (plotted in orange on the same figure) and matches the theoretically-predicted behavior of pathloss from §4.2.
- The SNR trend with depth demonstrates the superiority of TARF over a pure RF communication link. In particular, RF signals in the GHz range decay exponentially at a rate of around 1000 dB/m in seawater [24, 29].
- TARF’s recorded SNR displayed some variation from the expected trend. This is due to noise and interference from waves caused by swimmers and water circulation cycles.

(b) SNR vs Alignment. Our experiments so far have focused on scenarios where the transmitter and the receiver are aligned along the same (vertical) axis to maximize the SNR. Next, we evaluated TARF’s performance with varying degrees of misalignment. We performed this evaluation in the water tank setup, where we placed the radar 20 cm above the water surface and placed the speaker 40 cm below the surface. To understand TARF’s performance as a function of different alignments, we varied the speaker’s location at different horizontal displacements in the plane parallel to the water surface.

Fig. 12 plots the computed mean and standard deviation of the SNR as a function of the horizontal displacement between the underwater speaker and the FMCW radar. The figure shows that the SNR decreases from 11 dB when the transmitter and receiver are vertically aligned to around 3 dB when the horizontal misalignment is around 28 cm. Interestingly, the degradation is less than 10dB within a disk of diameter about half a meter. It is important to note, however, that this SNR degradation is dependent on the beam profiles of both the acoustic transmitter and FMCW radar.

8.3 Robustness to Waves

Lastly, we are interested in investigating TARF’s performance in the presence of surface waves. In particular, because TARF communicates by measuring minute vibrations on the water surface, we expect naturally occurring waves to interfere with

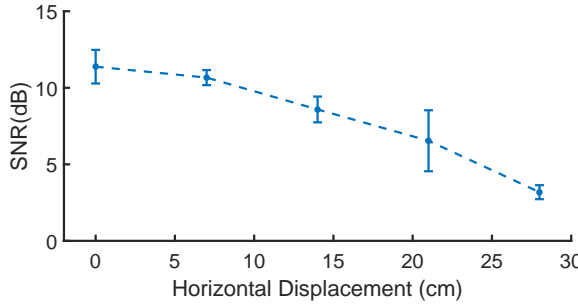


Figure 12—SNR vs Misalignment. The figure shows that Tarf’s SNR degrades as a function of the horizontal misalignment between the transmitter and the receiver. Error bars indicate standard deviation.

the communication signals. Hence, we would like to evaluate the effectiveness of Tarf’s interference cancellation in dealing with these waves. To this end, we performed controlled evaluation in the water tank, where we fixed the FMCW radar 30cm above the water surface and fixed the speaker 30cm below the surface. In order to quantify the effect of waves with our system, we emulate naturally occurring waves by creating 2Hz – 3Hz waves [58] at different peak-to-peak amplitudes and perform Tarf communication with BPSK modulation. Waves were generated manually as described in §7, and their amplitudes were measured with a graded ruler. We estimate the uncertainty in our wave amplitude measurement to be of the order of 1 cm.

Fig. 13 plots the mean and standard deviation of the throughput as a function of the peak-to-peak amplitude. We make the following observations:

- Tarf’s channel maintained minimal degradation up to 6 cm waves, which are 100,000× larger than the surface vibrations caused by the underwater acoustic transmitter, as observed in Fig. 3(a). Tarf’s ability to deal with this large interference arises from its unwrapping and filtering stages, which significantly mitigate the slower moving waves.
- For waves whose peak-to-peak amplitude is 22 cm or larger, Tarf’s throughput drops to zero. Multiple factors that contribute to this performance. First, the phase wraps too quickly for the unwrapping stage to reliably unwrap it. And second, larger waves may deflect the radar reflection away from our receiver (due to radio waves’ partially specular nature), leading to a reduction in the overall SNR.

9 LIMITATIONS AND OPPORTUNITIES

This paper presents Tarf, the first technology that enables underwater sensors to wirelessly communicate with compact airborne nodes. Tarf transforms the water-air boundary, which has been traditionally considered an obstacle for communication, itself into a communication interface. As such, it holds promise to solve the long-standing problem of cross-medium communications.

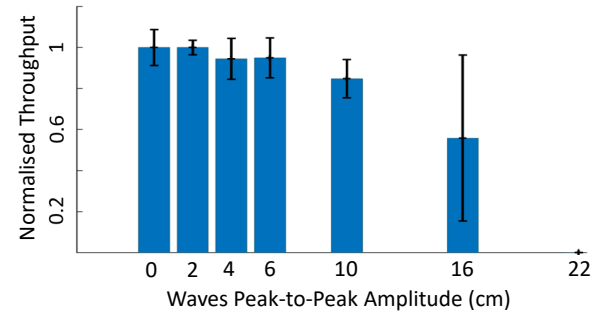


Figure 13—Throughput vs Surface Wave Amplitude. Tarf’s throughput decreases in the presence of interference from surface waves. Error bars indicate standard deviation.

Below, we highlight some of Tarf’s key limitations and potential development opportunities:

- *One-directional Communication:* Tarf only enables up-link communication from the underwater sensor to an airborne node. As described in §3, this limits the scope of the design, but still opens up many exciting applications in the underwater networking.
- *Ocean Wave Amplitude:* Our current prototype can sustain a communication link in the presence of surface waves with peak-to-peak amplitudes up to 16 cm. It is desirable to extend Tarf to operate with stronger waves and inclement weather conditions. One promising approach is to actively track the surface waves by both the transmitter and receiver and adapt the communication protocol accordingly.
- *Misalignment:* Our evaluation has demonstrated that Tarf’s performance degrades when the transmitter and receiver are misaligned. As a result, an airborne Tarf receiver will need to finely scan the water surface in order to localize the underwater transmitter. This limitation may be mitigated by innovative scanning solutions that adapt the beam profiles of both the acoustic and radar devices with height, depth, and expected SNR.

Despite these limitations, we believe that Tarf marks an important step toward practical and scalable cross-medium communications. It can enable many applications including submarine-to-drone communication, deep-sea exploration, and subsea IoT (Internet of Things). We hope that this paper will motivate researchers to explore Tarf as a means to enable truly ubiquitous communication across boundaries.

Acknowledgments. We thank Nanette Wu, Alex Sludds, Harry Hsu, and Ali Zartash for helping with the experiments, and thank Yunfei Ma for his help in designing the FMCW radar. We also thank Thomas Consi and Michael Sacarny from the MIT Sea Grant for their help in the setup, and Katy Croff Bell from the MIT Open Ocean initiative for helpful discussions. Finally, we thank Unsoo Ha, our shepherd Aaron Schulman, and the anonymous SIGCOMM reviewers for their helpful feedback on the manuscript. This research is partially supported by the MIT Media Lab and the NSF.

REFERENCES

- [1] 2017. <https://www.performanceaudio.com/item/electro-voice-uw30-underwater-loudspeaker/41594/>. (2017).
- [2] 2017. <https://www.outdoorspeakerdepot.com/75w-sub-amp-150w-in-wall-subwoofwe.html>. (2017).
- [3] 2017. <http://www.pyleaudio.com/sku/PT270AIU/300-Watt-Stereo-Receiver-with-Built-In-iPod-Docking-Station-AM-FM-Tuner,-USB-Flash-and-SD-Card-Readers-and-Subwoofer-Control>. (2017).
- [4] 2017. <https://www.sagemillimeter.com/23-dbi-gain-wr-15-v-band-rectangular-horn-antenna/>. (2017).
- [5] 2017. usrp n210. <http://www.ettus.com>. (2017). ettus inc.
- [6] Fadel Adib, Zachary Kabelac, Dina Katabi, and Robert C. Miller. 2014. 3D Tracking via Body Radio Reflections. In *Usenix NSDI*.
- [7] Fadel Adib, Zachary Kabelac, Hongzi Mao, Dina Katabi, and Robert C Miller. 2014. Real-time breath monitoring using wireless signals. In *Proceedings of the 20th annual international conference on Mobile computing and networking*. ACM, 261–262.
- [8] Ian F Akyildiz, Dario Pompili, and Tommaso Melodia. 2005. Underwater acoustic sensor networks: research challenges. *Ad hoc networks* 3, 3 (2005), 257–279.
- [9] Steven L Bernstein, Michael L Burrows, James E Evans, AS Griffiths, DA McNeill, CW Niessen, I Richer, DP White, and DK Willim. 1974. Long-range communications at extremely low frequencies. *Proc. IEEE* 62, 3 (1974), 292–312.
- [10] D Brumbi. 2000. Low power FMCW radar system for level gaging. In *Microwave Symposium Digest. 2000 IEEE MTT-S International*, Vol. 3. IEEE, 1559–1562.
- [11] W. S. Burdic. 1991. *Underwater acoustic system analysis*. NJ: Prentice Hall.
- [12] Xianhui Che, Ian Wells, Gordon Dickers, Paul Kear, and Xiaochun Gong. 2010. Re-evaluation of RF electromagnetic communication in underwater sensor networks. *IEEE Communications Magazine* 48, 12 (2010), 143–151.
- [13] Xianhui Che, Ian Wells, Gordon Dickers, Paul Kear, and Xiaochun Gong. 2010. Re-evaluation of RF electromagnetic communication in underwater sensor networks. *IEEE Communications Magazine* 48, 12 (2010), 143–151.
- [14] Steven Constable. 2010. Ten years of marine CSEM for hydrocarbon exploration. *Geophysics* 75, 5 (2010), 75A67–75A81.
- [15] Caraivan Mitruț Cornelius, Dache Valentin, and Sgărciu Valentin. 2012. Deploying Underwater Sensors Safe-Net in Offshore Drilling Operations Surrounding Areas Using Remote Operated Vehicles. *IFAC Proceedings Volumes* 45, 6 (2012), 871–876.
- [16] Wang C. J. Wen B. Y. Ma Z. G. Yan W. D. and Huang X. J. 2007. Measurement of river surface currents with UHF FMCW radar systems. *Journal of Electromagnetic Waves and Applications* (2007).
- [17] Mari Carmen Domingo. 2011. Securing underwater wireless communication networks. *IEEE Wireless Communications* 18, 1 (2011).
- [18] Matthew Dunbabin, Peter Corke, and Gregg Buskey. 2004. Low-cost vision-based AUV guidance system for reef navigation. In *Robotics and Automation, 2004. Proceedings. ICRA'04. 2004 IEEE International Conference on*, Vol. 1. IEEE, 7–12.
- [19] CR Grant and BS Yaplee. 1957. Back scattering from water and land at centimeter and millimeter wavelengths. *Proceedings of the IRE* 45, 7 (1957), 976–982.
- [20] Aditya Gudipati and Sachin Katti. 2011. Strider: Automatic rate adaptation and collision handling. In *ACM SIGCOMM Computer Communication Review*, Vol. 41. ACM, 158–169.
- [21] Aditya Gudipati, Stephanie Pereira, and Sachin Katti. 2012. AutoMAC: Rateless wireless concurrent medium access. In *Proceedings of the 18th annual international conference on Mobile computing and networking*.
- [22] Daniel Halperin, Wenjun Hu, Anmol Sheth, and David Wetherall. 2010. Predictable 802.11 packet delivery from wireless channel measurements. In *ACM SIGCOMM Computer Communication Review*, Vol. 40. ACM, 159–170.
- [23] Duo-Min He. 1999. High-power Nd: YAG-generated underwater sound source for air-submarine communication. In *Solid State Lasers VIII*, Vol. 3613. International Society for Optics and Photonics, 83–93.
- [24] EJ Hilliard Jr. 1960. *Electromagnetic Radiation in Sea Water*. Technical Report. Naval Underwater Ordnance Station Newport RI.
- [25] David Hoffman. 2009. *The Dead Hand: The Untold Story of the Cold War Arms Race and Its Dangerous Legacy*. Anchor.
- [26] Ling Ji, Jun Gao, Ai-Lin Yang, Zhen Feng, Xiao-Feng Lin, Zhong-Gen Li, and Xian-Min Jin. 2017. Towards quantum communications in free-space seawater. *Optics Express* 25, 17 (2017), 19795–19806.
- [27] Balakrishnan Kaushik, Don Nance, and Krish Ahuja. 2005. A review of the role of acoustic sensors in the modern battlefield. In *11th AIAA/CEAS Aeroacoustics Conference*. 2997.
- [28] Peter Kimball and Stephen Rock. 2008. Sonar-based iceberg-relative AUV navigation. In *Autonomous Underwater Vehicles, 2008. AUV 2008. IEEE/OES*. IEEE, 1–6.
- [29] Liu Lanbo, Zhou Shengli, and Cui Jun-Hong. 2008. Prospects and problems of wireless communication for underwater sensor networks. *Wireless Communications and Mobile Computing* 8, 8 (2008), 977–994.
- [30] Fill Youb Lee, Bong Huan Jun, Pan Mook Lee, and Kihun Kim. 2008. Implementation and test of ISI-MI100 AUV for a member of AUVs Fleet. In *OCEANS 2008*. IEEE, 1–6.
- [31] Yingzhuang Liu and Xiaohu Ge. 2006. Underwater laser sensor network: A new approach for broadband communication in the underwater. In *Proceedings of the 5th WSEAS International Conference on Telecommunications and Informatics*. 421–425.
- [32] Xavier Lurton. 2002. *An introduction to underwater acoustics: principles and applications*. Springer Science & Business Media.
- [33] Xavier Lurton. 2002. *An introduction to underwater acoustics: principles and applications*. Springer Science & Business Media.
- [34] G Meinecke, V Ratmeyer, and G Wefer. 1999. Bi-directional communication into the deep ocean based on ORBCOMM satellite transmission and acoustic underwater communication. In *OCEANS'99 MTS/IEEE. Riding the Crest into the 21st Century*, Vol. 3. IEEE, 1405–1409.
- [35] Michael V Namorato. 2000. A concise history of acoustics in warfare. *Applied Acoustics* 59, 2 (2000), 101–135.
- [36] David Pearson, Edgar An, Manhar Dhanak, Karl von Ellenrieder, and Pierre Beaujean. 2014. *High-level fuzzy logic guidance system for an unmanned surface vehicle (USV) tasked to perform autonomous launch and recovery (ALR) of an autonomous underwater vehicle (AUV)*. IEEE.
- [37] Jeffery J Puschell, Robert J Giannaris, and Larry Stotts. 1992. The autonomous data optical relay experiment: first two way laser communication between an aircraft and submarine. In *Telesystems Conference, 1992. NTC-92., National*. IEEE, 14–27.
- [38] Hariharan Rahul, Farinaz Edalat, Dina Katabi, and Charles G Sodini. 2009. Frequency-aware rate adaptation and MAC protocols. In *Proceedings of the 15th annual international conference on Mobile computing and networking*. ACM, 193–204.
- [39] Shobha Sundar Ram and Hao Ling. 2008. Through-wall tracking of human movers using joint Doppler and array processing. *IEEE Geoscience and Remote Sensing Letters* 5, 3 (2008), 537–541.
- [40] Mark Rhodes, Derek Wolfe, and Brendan Hyland. 2011. Underwater communications system comprising relay transceiver. (2011). US Patent 7,877,059.
- [41] H Rowe. 1974. Extremely low frequency (ELF) communication to submarines. *IEEE Transactions on Communications* 22, 4 (1974),

- 371–385.
- [42] Manecius Selvakumar, Ramesh R Subramanian, AN Sathianarayanan, D Harikrishnan, G Jayakumar, VK Muthukumaran, D Murugesan, M Chandrasekaran, E Elangovan, Doss Prakash, et al. 2010. Technology tool for deep ocean exploration-remotely operated vehicle. In *Proceedings of the 20th International Offshore and Polar Engineering Conference, Beijing, China*. 206–212.
 - [43] Robert H Stewart. 2008. *Introduction to physical oceanography*. Robert H. Stewart.
 - [44] Milica Stojanovic. 1995. Underwater acoustic communications. In *Electro/95 International. Professional Program Proceedings*. IEEE, 435–440.
 - [45] Milica Stojanovic. 2007. On the relationship between capacity and distance in an underwater acoustic communication channel. *ACM SIGMOBILE Mobile Computing and Communications Review* 11, 4 (2007), 34–43.
 - [46] M. Stojanovic. 2007. On the relationship between capacity and distance in an underwater acoustic communication channel. In *SIGMOBILE Mobile Computing and Communications Review*. ACM, 34–43.
 - [47] Andrew G Stove. 1992. Linear FMCW radar techniques. In *IEE Proceedings F (Radar and Signal Processing)*, Vol. 139. IET, 343–350.
 - [48] Kuan Meng Tan, Tommie Liddy, Amir Anvar, and Tien-Fu Lu. 2008. The advancement of an autonomous underwater vehicle (AUV) technology. In *Industrial Electronics and Applications, 2008. ICIEA 2008. 3rd IEEE Conference on*. IEEE, 336–341.
 - [49] Paul J Titterton, Frederick Martin, Dan J Radecki, and Robert W Cotterman. 1991. Secure two-way submarine communication system. (Aug. 6 1991). US Patent 5,038,406.
 - [50] David Tse and Pramod Viswanath. 2005. *Fundamentals of wireless communication*. Cambridge university press.
 - [51] EJ Tucholski and S Traffic. 2006. Underwater Acoustics and Sonar. SP411 Handouts and Notes. Fall 2006. *Physics Department, US Naval Academy* 12 (2006), 11–1.
 - [52] Lloyd Butler VK5BR. 1987. Underwater radio communication. *Originally published in Amateur Radio* (1987).
 - [53] John G Webster and Halit Eren. 2017. *Measurement, instrumentation, and sensors handbook: spatial, mechanical, thermal, and radiation measurement*. CRC press.
 - [54] Louis Whitcomb, Dana R Yoerger, Hanumant Singh, and Jonathan Howland. 2000. Advances in underwater robot vehicles for deep ocean exploration: Navigation, control, and survey operations. In *Robotics Research*. Springer, 439–448.
 - [55] T Wiener and Sherman Karp. 1980. The role of blue/green laser systems in strategic submarine communications. *IEEE Transactions on Communications* 28, 9 (1980), 1602–1607.
 - [56] S Wolf, J Davis, and M Nisenoff. 1974. Superconducting extremely low frequency (ELF) magnetic field sensors for submarine communications. *IEEE Transactions on Communications* 22, 4 (1974), 549–554.
 - [57] Robert Woodall, Felipe Garcia, and John Sojdehei. 2000. Magneto-inductive submarine communications system and buoy. (May 2 2000). US Patent 6,058,071.
 - [58] I. R. Young. 1999. *Wind generated ocean waves (Vol. 2)*. Elsevier.
 - [59] Ju Zhang, Xiaoping Zhu, and Zhou Zhou. 2010. Design of time delayed control systems in UAV using model based predictive algorithm. In *Informatics in Control, Automation and Robotics (CAR), 2010 2nd International Asia Conference on*. IEEE, 269–272.
 - [60] Shengli Zhou and Zhaohui Wang. 2014. *OFDM for underwater acoustic communications*. John Wiley & Sons.